Accurate Focus Correction for Large Telescopes

Richard Holmes
Boeing LTS, 550 Lipoa Parkway, Kihei, HI, 96753
Brett Sickmiller
Leidos, Inc., Albuquerque, NM 96753
Nicholas Steinhoff
the Optical Sciences Company, P. O. B. 25309, Anaheim, CA 92825
Skip Williams
Air Force Research Laboratory, 550 Lipoa Parkway, Kihei, HI, 96753
Andrew Whiting
Boeing LTS, 550 Lipoa Parkway, Kihei, HI, 96753

ABSTRACT

A ubiquitous issue in observations with large telescopes is focus control. Typical auto-focus algorithms used in commercial cameras are not effective for the astronomical application due to the long range to space objects and the random focus caused by atmospheric turbulence. Focus can be mitigated with an adaptive optics system. However, adaptive optics systems are typically complex and costly, and adaptive optics based on an artificial beacon will not usually sense or correct for focus. This paper discusses alternative approaches that are relatively low in cost and complexity. These options include means based on a tracker/imager, as well as a dedicated focus sensor. The dedicated focus sensor is a simplified form of a Hartmann wavefront sensor (WFS). The specific implementation of such a focus sensor will be shown to provide significant benefits for focus correction. The tracker/imager-based implementations have an intrinsic ambiguity of the sign of the focus, due to the nature of focus sensed on an image plane. However, this ambiguity can be overcome with careful algorithm design, or with hardware modifications described below. Three primary options are considered for tracker/imager-based focus control: an autofocus metric, a spot-width-estimation algorithm, and an approach that enables direct estimation of the sign of the focus via a fixed astigmatism aberration. It is found that the spot-width estimation algorithm works nearly as well as a dedicated focus sensor, with rapid resolution of the sign ambiguity. In addition to performance, top-level cost and implementation issues are also considered for generic telescope systems with apertures greater than 0.5 meters.

1. INTRODUCTION

Focus is a common error on telescopes, impacting both image formation as well as object detection. The optical path is not the only source of focus error; focus and astigmatism represent 52 % of the atmospheric phase aberrations after piston, tip, and tilt are removed [1].

Hence, correction of focus is desirable, and preferably without the complexity of adaptive optics. However, focus control is also important when using artificial beacons with adaptive optics. This is because backscatter from a guidestar beacon will have a large focus due to the backscatter range, which makes it difficult to sense or correct for the relatively small atmospheric focus that is added in. This backscatter range is typically not well-known, so focus is un-sensed with such beacons. Focus anisoplanatism is also an issue even if the backscatter range were well-known. The objective herein is to consider several options for focus control. Several approaches concepts are evaluated in terms of accuracy, cost, and complexity. Object brightness is also a consideration but will not be discussed in detail. The emphasis will be on the use of un-resolved sources in the scene.

2. FOCUS SENSING CONCEPTS

Four basic versions of focus sensing are considered. All approaches are based on signal from an object of interest or some other object that is in the scene that is preferably unresolved. The first approach uses a wavefront sensor (WFS) with large subapertures. A WFS with 2x2 subapertures in the pupil plane is sufficient to measure focus and both components of astigmatism without any ambiguity. An implementation comprising a 2x2 Hartmann WFS is shown schematically in Fig. 1 on the far left. The other three approaches are based on a tracker image of the object

or scene of interest. The simplest approach is to just measure the spot width of point-like object in the scene [2]. The overall spot width is a measure of defocus. Measurement of spot width in the 3 different radial directions will produce estimates of two components of astigmatism as well. This approach is shown second from left in Fig. 1. Third from left is also a tracker-based approach, in which the scene contrast is used as a metric for focus. This approach was selected as best among about 18 different algorithms used for camera auto-focus [3]. This algorithm does not compute the astigmatisms however. This approach is shown third from left in Fig. 1. Fourth and last among the approaches considered is a tracker-based approach in which astigmatism is deliberately added to the wavefront, just in front of the focusing lens [4]. This approach allows identification of positive and negative focus, by observing the direction of the ellipticity of the spot on the tracker as a function of focus. It's possible that the tracker/imager based approaches can sense the two components of astigmatism as well, but that is beyond the scope of this effort. A more detailed discussion of these approaches is now presented.

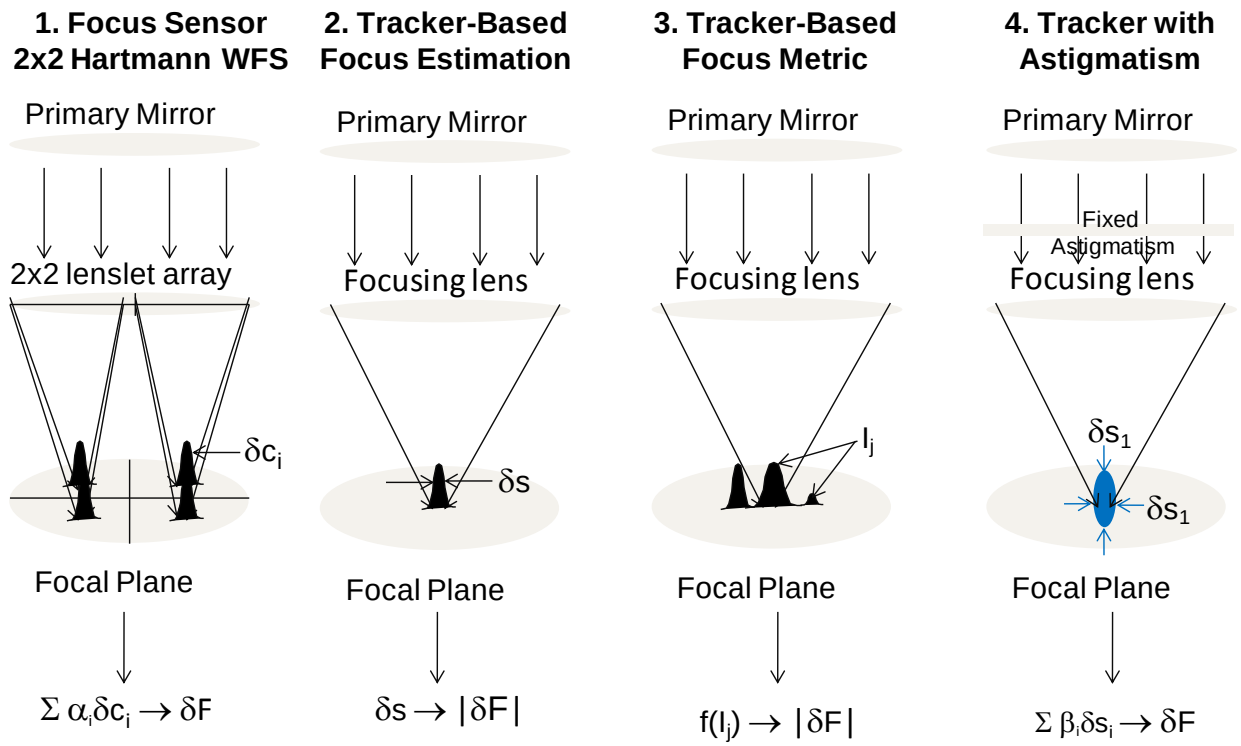

Fig. 1. Focus Correction Approaches.

The first approach, referred to as a "focus sensor," involves a wavefront sensor. An array of 2x2 subapertures in a Shack-Hartmann sensor configuration will produce a set of 2x2 x-y centroids, and so is capable of measuring 8 degrees of freedom of the wavefront. These degrees of freedom include focus and both astigmatism aberrations. Focus is computed in this approach using a weighted sum of these 8 numbers, and the choice of a very simple algorithm (least-mean-square), seems to work well. The approach does suffer some degradation when the spots in each subaperture are not well formed, as may occur when turbulence is relatively strong or not well corrected by the AO system.

The second approach is referred to as tracker-based focus estimation" (TBFE). In this approach, the measured size of spot on the focal plane is compared to a nominal spot size, and the difference is used to estimate the residual focus. The choice of the nominal spot size is important, because any bias in this "null" value will result in a constant error that feeds into the type I filter used to estimate the focus, causing a growing error. To overcome this, the null value of spot or object width is estimated using a boxcar average of the focus in excess of the diffraction limited focus. In the absence of initial focus correction, this will tend to initially over-estimate the focus null, and so under-estimate focus. To address this, the focus null estimate is set to a fraction of the raw focus null estimate summed in quadrature with the defocus associated with the diffraction-limited spot. This in turn will cause some

slightly aggressive correction of focus that can self-correct in the loop, since over-correction will ultimately result in a larger spot that will result in an estimate of the null that is slightly larger. Also, this focus null can vary over time as the degree of AO correction (excluding focus) improves or degrades.

In addition to estimation of the null spot width, there is a second issue of the sign of the focus. As shown in Fig. 2, the sign of the focus cannot be intrinsically determined from a simple focal plane measurement. To address this, a software approach initially involves applying the full amount of estimated focus in a positive sense. If the result of this application causes the spot size to increase, then the algorithm assumes that the initial sign of the focus is incorrect and applies a focus of the opposite sign. This process will almost always causes the measured spot width to decrease. Then if the focus residual eventually grows larger than the focus estimate, the sign of the gain factor is reversed and reduced. If this fails to reduce the error, then the focus estimate is again switched in sign. These dither-like steps minimize error in the sign and have proven to reduce focus error.

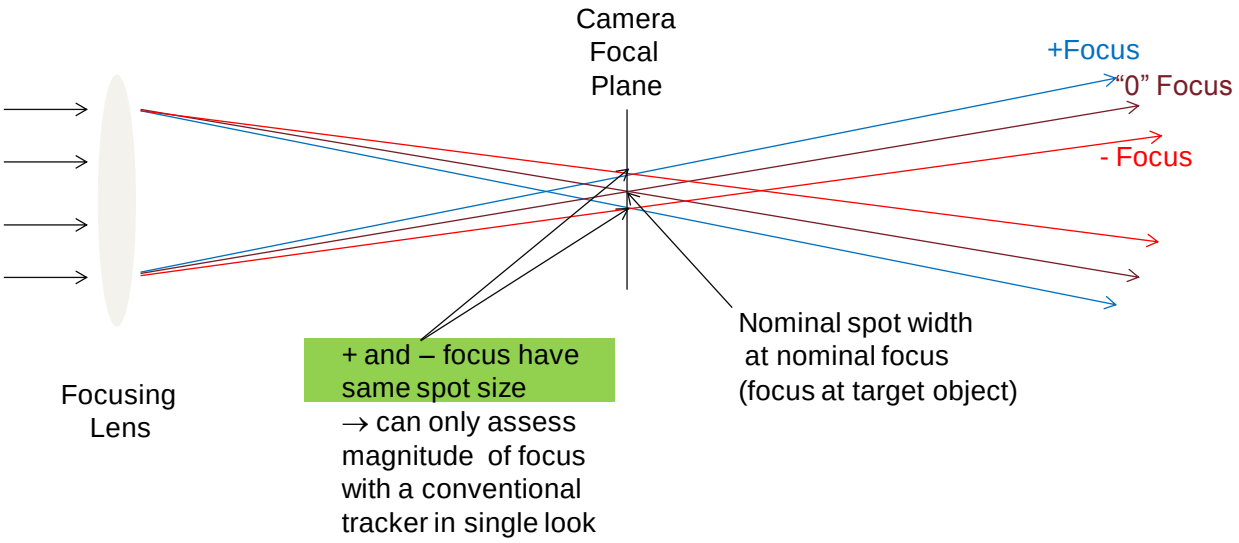

Fig. 2. Intrinsic sign ambiguity of focus in tracker data.

A third technique explored is called the "Tracker-based Focus Metric"(TBFM). This approach computes a simple metric that is correlated to focus. This metric was selected based on past studies of auto-focus for consumer cameras [4]. The basic idea is to minimize focus error by maximizing the metric. The metric was the best or nearly the best of roughly18 different metrics considered ("best" depends on the scene considered). Ease of implementation was also considered in the selection of this metric, which is simply

$$\Sigma_i \, p(x_i)|x_i-\mu| \qquad (1)$$

where μ is the mean value of the scene, x_i is the mean value of pixels given range of signal levels, and $p(x_i)$ is the probability (frequency) of those pixels. The parameter $p(x_i)$ varies over the range of signal levels x_i in the scene. The number in 1 represents the mean of the absolute value of the first moment of the pixel signal distribution. The idea is that if the image is defocused, more signal levels will be similar, so it is better to create a large variation in signal levels. To perform this maximization, a secant method was added to the maximization, and the logic used for TBFE was also used to address sign errors. The problem with this algorithm is that it proved to be sensitive to noise when the best focus is near infinity (inverse focus near zero), and the selection of the "scene" region is not obvious.

The fourth technique, "Tracker with Added Astigmatism", is a clear means to extract the sign of the focus from a tracker by deliberately adding astigmatism to the incoming light. If focus were the only aberration on the incoming light, and sufficient astigmatism were added in the beam path, then adding focus will cause a spot ellipticity in one direction on the focal plane, and subtracting focus will cause a change in spot ellipticity in the orthogonal direction

[5]. To eliminate the impact of a resolved object, a second leg is used with the addition of astigmatism of opposite sign, and the result of the second leg can be subtracted from the first leg.

The above approaches are sometimes compared herein to an idealized approach, in which the focus is sensed from an idealized sodium beacon (a single thin layer). In such cases, the focus due to the beacon range is removed and one is left with an estimate of atmospheric and beam train focus from the beacon. This idealized beacon is located at a nominal 9 microradian lead-ahead angle. 9 microradians is chosen for latency and pt-ahead considerations. Hence in these cases the sodium beacon return will have as error sources (a) both the focus part of the focus anisoplanatism of the beacon source at 90 km, as well as (b) the focus part of conventional angular anisoplanatism.

3. CONCEPT EVALUATION

The basic approach uses a wave-optics simulation to evaluate performance. Two independent wave-optics simulations were used to reduce the likelihood of errors of any kind in the final result. The results of the two codes were compared and found to agree to within about 10%, so the overall results are considered to have reasonable accuracy. The simulation considered a series of tests that lead up to the full simulation in HELFire, and then confirmational simulations with SimISAL. The series of tests include (a) focus-only aberration, (b) focus + atmospheric turbulence at 35degrees zenith, (c) use of a target beacon for AO, (d) finally use of a sodium beacon for AO. All these cases were run with a 3.63 meter telescope. Cases were also run 1.5 meter telescope with the sodium beacon and cases were run with a 1 meter telescope, no AO correction. The cases also consider objects that are nearly unresolved.

Table 1 shows a summary of the input conditions. The approach uses with propagation through the atmosphere and the beam train, with a ~ 1 cm grid resolution, and 1024x1024 grids. Propagation through turbulence in these uplooking geometries uses 10 phase screens and Fresnel propagation between screens with the standard split-operator approach. A detailed model of beam train is also included.

Table 1. Summary of simulation conditions.

Parameter	Value
Propagation grid in atmosphere	1024 x 1024
Propagation grid in beam path	512 x 512
Propagation grid-point spacing	1 cm
Turbulence Model	1 x Maui3, at Haleakala site
Number of phase screens	10, at locations appropriate for upward propagation
Target Altitude above MSL	800 km (LEO) 36,000 km (GEO)
Target Range	948 km (LEO) 36,993 km (GEO)
Number of time steps	initially 100 steps at 1 KHz (0.1 sec total duration)
Zenith Angle	35 degrees
Target brightness	12 Mv for tracker
Strength of focus aberration	670 nm peak-valley, corresponds to F = 2.5 Mm
Primary Mirror Aperture Sizes	3.63 meters, 1.5 meters (1.0 meters no wavefront control)
DM model	177 actuators, 13 actuators across primary mirror, edge-edge Corresponds to good correction for 1.5 meter aperture, under-correction for 3.63 meter aperture
WFS configuration	12 x 12 subapertures, 8 x 8 pixels / subaperture
WFS wavelength	589 nm
WFS pixel FOV	3 microradians in output space

For the cases in which AO is used, there are 2 pupil relays; the first relay transfers light from the pupil onto the DM with telecentric imaging and the second relay telecentrically transfers the light from the DM onto the wavefront sensor. A detailed model of control system (but with reduced latency in some cases) is used. An accurate model of wavefront reconstruction process is used. A reconstructor is generated, based on poke test, followed by inversion with waffle constraint, and then piston, tip, tilt (and focus for artificial beacon) are removed over active actuators, followed by slaving of inactive actuators. The simulations also include realistic sensor models, with noise and saturation (though saturation had no effect in the model runs). There is also some idealization of actuator temporal response and beacon sources. Point source artificial beacons are used, although sensitivity to more realistic extended beacons was explored. High signal levels were assumed for the beacon WFS, Mv=12 was assumed for the tracker.

Table 2. Performance of different focus approaches under different focus/atmospheric/beacon conditions. Results are shown for 589 nm / 800 nm.

Conditions → Control System ↓	**Focus Aberration Only, Target Beacon**	**Atmosphere + Focus, Target Beacon**	**Focus Aberration Only, LGS beacon**	**Atmosphere + Focus, LGS beacon**
AO + Focus Sensor	**0.98 / 0.99+**	**0.052 / 0.36**	**0.95 / 0.99+**	**0.032 / 0.17**
AO + Tracker-Based Focus Estimation	**0.89 / 0.99+**	**0.051 / 0.36**	**0.96 / 0.99+**	**0.030 / 0.15**
AO + Tracker-Based Focus Metric	**0.57 / 0.97**	**0.0034 / 0.028**	**0.95 / 0.88**	**0.0040 / 0.032**
AO + AO from beacon (idealized)	**0.98 / 0.99+**	**0.063 / 0.35**	**0.97 / 0.99+ (*)**	**0.031 / 0.17 (*)**

(*) LGS results are with a single backscatter layer and a point beacon, and with a low-gain focus-adjust trombone in place.

Table 2 shows the performance of the three basic techniques. The top row shows the focus sensor (FS) results, and it seems to perform somewhat better than the tracker-based focus estimation (TBFE) results on row two. Since these two rows show relatively good (and similar) performance, they are marked in green. Row 3 shows the TBFM results, and these are definitely degraded compared to the FS and TBFE results shown above. The last row shows results for when the beacon WFS is used to remove focus, with an idealized single-layer beacon. Even this idealized beacon WFS is not a perfect corrector of focus when a sodium Laser Guidestar (LGS) beacon is used, due to both angular anisoplanatism and focus anisoplanatism. The first and third data columns show good performance, as expected, because the only aberration is a static focus (described in Table 1) in the beam train. The second data column of Table 3, with target beacon, is most relevant for the AEOS telescope for bright targets, for low-density actuator spacing. The last data column is most relevant for AEOS for dim targets for low-density actuator spacing, and shows reduced performance, accordingly, compared to the target beacon.

Figs. 4 and 5 show sample data sets of Strehl versus time, to understand not only the mean Strehl but also the variations. Fig. 4 shows the average of 10 realizations at each time step, with a time average peak strehl of 0.17 for FS, and a time average peak strehl of 0.16 for TBFE. The tracker sample rate is 300 Hz, so the durations have many samples over a run duration. The mean Strehls are computed after about 15 msec from the start of the run, to properly characterize steady-state performance. The figures show comparable performance of the focus sensor and the tracker-based focus estimation approaches, and slightly less than that of an idealized LGS beacon.

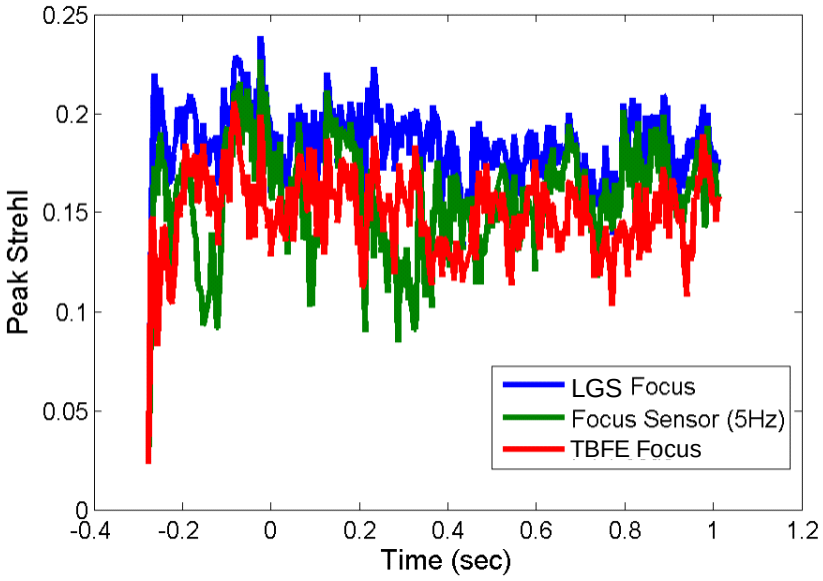

Fig. 3. Realization-averaged time history of peak strehl on at tracker/imager at 800 nm with three different focus correction approaches (average over 10 realizations, each of duration 1.25 sec).

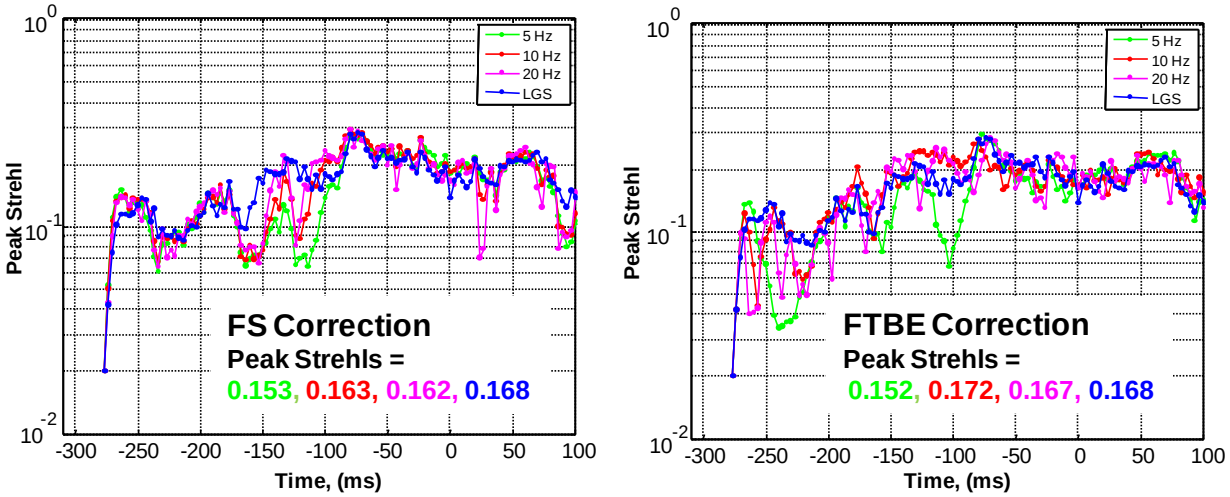

Fig. 4. Impact of varying digital filter bandwidth for focus sensor (left) and tracker-based focus estimation (right), showing peak strehl versus time for a tracker/imager of at 800 nm. A single turbulence/noise realization is used in both cases.

4. TOP LEVEL IMPLEMENTATION ISSUES

The FS approach is found to be most robust, but does have some sensitivity to the quality of AO compensation. The more robust design requires Nyquist sampling in the focal plane, and a relatively large subaperture FOV to ensure spots are captured. The second approach considered in detail herein is the TBFE approach. It performs a bit worse than the FS. It has the issue of +/- focus ambiguity, but the algorithms address this fairly well, by switching sign of focus correction if the measured focus increases upon application of the correction. It also has the issue of sensitivity to the size of the AO-compensated spot width, which is addressed by a separate spot-width estimation process. The TBFE approach degrades if the pixel FOV is greater than Nyquist sampling (pixel FOV > 0.5λ/D). A large pixel FOV introduces a bias in spot width and hence focus measurement, which can be handled by estimating the spot-width as discussed above, if the pixel size is not too much greater than Nyquist. In this case there is increased sensitivity to centering of the spot, which should nominally be at center of 2x2 pixels. TBFE with deliberately

added astigmatism is also expected to work fairly well, better that TBFE alone, because of its sensitivity to the sign of the focus error. The last approach considered, TBFM, is least robust. The best or near-best commercial camera algorithm was used for a scene-based focus estimate. Sim experience, shown above, as well as discussions with amateur astronomers, indicates that camera auto-focus algorithms do poorly against objects at infinity in the presence of turbulence. The TBFM approach also has some of the issues listed above that were observed with TBFE.

The above discussions pertain to primarily to accuracy performance of the approaches. What about cost and complexity of the approaches? The focus sensor approach does require a separate sensor, and this sensor will work best when the pixel size matches the angular Nyquist sampling criterion. In this case, Nyquist sampling is $0.5\lambda/D_{subap}$, where λ is the wavelength, and D_{subap} is the subaperture width, which in this case is ½ the aperture width. In addition, many pixels across subapertures are typically required to obtain an acceptable field-of-view. Given this, the focus sensor may require tens to hundreds of pixels across the array, and so is consistent with a focal plane implementation. Hence, the FS focal plane and associated real-time processing would incur additional cost and complexity for focus estimation. Also, the FS approach will require its own spectral band, which removes photons from other bands. It should be noted that the focus sensor can also provide tilt information, so it could be used in place of a tracker, but would have somewhat reduced sensitivity since the light is divided into 4 subapertures. Finally, the FS approach can be generalized to also correct for astigmatism, and it seems to be a bit more robust based on the time histories of the previous section.

The TBFE does *not* require an extra sensor, nor does it require a separate spectral band. However, the approach has additional processing complexity, and there are some restrictions on the pixel size (preferably Nyquist sampling or better as mentioned above). The performance with extended objects may be degraded. To address this and the sign of the focus, the addition of astigmatism into the beam path may be used, and this is only a small modification to the optical path. The use of two parts of the same camera for the two signs of the astigmatism represents a non-trivial additional hardware and processing cost. The light from the target will also be spread among more pixels, due to both the use of astigmatism as well as the second astigmatism of inverted sign. These issues are not addressed herein but left for future work.

5. POTENTIAL APPLICATIONS

Based on the above evaluations, one can see value in focus correction of generic telescope systems with apertures greater than about 0.5 meters. In particular, mid-sized telescopes with 40-100 cm apertures but without adaptive optics can benefit from this approach. The telescope itself can usually be used to correct focus, and astigmatism correction can be achieved with simple optical means. Such an approach can provide a low-cost approach to improve the signal-to-noise ratio for dim objects.

The focus sensor may be preferred over the other focus-sensing methods for mid-sized telescopes, if the best focus correction is more important than cost, and if no other higher-order wavefront control is utilized. TBFE will be lower cost.

For larger telescopes, which already have adaptive optics, the use of independent focus sensing has at least two benefits. First, it is useful to get object in focus, in the presence of telescope focus errors. This can improve acquisition of dim objects, as well as acquisition of the wavefront sensor data in which the wavefront sensor has limited angular acceptance angles. Second, as mentioned in the Introduction, artificial guidestars usually need a separate focus sensor for focus control, since the focus information is not usually available from the wavefront sensor measurements from an artificial beacon.

6. SUMMARY

Both a focus sensor and tracker-based approach perform fairly well, based on a wave-optics simulation. Both could be used to sense and correct astigmatism as well, with the focus sensor expected to have better sensitivity to such aberrations. The focus-sensor approach seems to be most robust in the presence of error sources such as camera noise and imperfect wavefront compensation. However, the focus sensor requires the added cost of a focal plane with Nyquist angular sampling for best performance.

Tracker-based focus estimation is nearly as good as the focus-sensor approach in the cases considered, but without the added cost of a separate Hartmann-Shack wavefront sensor. Some degradation occurs due to incorrect identification of the sign of the focus, contributing to a reduction of Strehl of about 10 % relative to the Strehl of the focus sensor in the simulation cases that were performed. TBFE also shows somewhat more sensitivity to camera parameters such as pixel field-of-view. The tracker-based approach can be augmented with a known fixed astigmatism in the optical path. This enables detection of the sign of the focus. However, such added astigmatism can obscure astigmatism sensing, and if significant astigmatism is present in the incoming wavefront, it can potentially confuse the estimate of focus.

Tracker-based focus metrics based on commercial auto-focus approaches were found to have difficulty with uplooking, long-range scenarios that typically involve larger telescopes. This comment is substantiated by amateur astronomers, who do not usually use camera auto-focus even though it is available, due to turbulence effects and a focus near infinity for space objects.

7. ACKNOWLEDGMENT

This work was funded by the Air Force Research Laboratory Contract # FA9451-05-C, Innovative Research and Optical Site Support. The U.S. Government is authorized to reproduce and distribute reprints for Governmental purposes notwithstanding any copyright notation thereon. The views and conclusions contained herein are those of the authors and should not be interpreted as necessarily representing the official policies or endorsements, either expressed or implied, of the Air Force Research Laboratory or the U.S. Government.

8. REFERENCES

1. Robert J. Noll, "Zernike polynomials and atmospheric turbulence, " *J. Opt. Soc. Am.* Vol. 66, 207-211 (1976).
2. R. Holmes, "Simulation of Focus Control," Technical Engineering Memo AO030, (2015).
3. R. Holmes, "Focus Control Architecture," Technical Engineering Memo AO011 (2013).
4. K. C. Meier, C. Pellizzari, A. Whiting, "A Comparison of Auto-focus Algorithms for Real-time Correction in SSA Imaging Systems," 10 July 2013, Technical Engineering Memo DP003 (2013).
5. J. Spinhirne, "Preliminary Design for the NGAS Astigmatic Focus Sensor," private communication, (July 2014).